The Journal of Chemical Physics

RESEARCH ARTICLE | SEPTEMBER 03 2024

Buffer gas cooled ice chemistry. II. Ice generation and mm-wave detection of molecules desorbed from an ice

T. J. Hager ; B. M. Moore ; Q. D. Borengasser ; A. C. Kanaherarachchi ; K. T. Renshaw; S. Radhakrishnan ; G. E. Hall ; B. M. Broderick

J. Chem. Phys. 161, 094201 (2024)
https://doi.org/10.1063/5.0225903
CHORUS

The Journal of Chemical Physics ARTICLE pubs.aip.org/aip/jcp

Buffer gas cooled ice chemistry. II. Ice generation and mm-wave detection of molecules desorbed from an ice

Cite as: J. Chem. Phys. 161, 094201 (2024); doi: 10.1063/5.0225903
Submitted: 26 June 2024 • Accepted: 15 August 2024 •
Published Online: 3 September 2024

T. J. Hager,[1] B. M. Moore,[1] Q. D. Borengasser,[1] A. C. Kanaherarachchi,[1] K. T. Renshaw,[1] S. Radhakrishnan,[1] G. E. Hall,[2] and B. M. Broderick[1,a)]

AFFILIATIONS

[1] Department of Chemistry, University of Missouri, Columbia, Missouri 65203, USA
[2] Brookhaven National Laboratory, Chemistry Division, Upton, New York 11973, USA

[a)] **Author to whom correspondence should be addressed:** broderickbm@missouri.edu

ABSTRACT

This second paper in a series of two describes the chirped-pulse ice apparatus that permits the detection of buffer gas cooled molecules desorbed from an energetically processed ice using broadband mm-wave rotational spectroscopy. Here, we detail the lower ice stage developed to generate ices at 4 K, which can then undergo energetic processing via UV/VUV photons or high-energy electrons and which ultimately enter the gas phase via temperature-programmed desorption (TPD). Over the course of TPD, the lower ice stage is interfaced with a buffer gas cooling cell that allows for sensitive detection via chirped-pulse rotational spectroscopy in the 60–90 GHz regime. In addition to a detailed description of the ice component of this apparatus, we show proof-of-principle experiments demonstrating the detection of H_2CO products formed through irradiation of neat methanol ices or 1:1 CO + CH_4 mixed ices.

I. INTRODUCTION

The cold and diffuse interstellar medium is surprisingly complex in its chemistry. Over 300 organic molecules, including complex organics (defined in the astrochemical sense as a molecule containing a minimum of six atoms), have been detected in cold dense interstellar molecular clouds.[1,2] Previously, this region of space was deemed too harsh an environment for the formation of complex molecules due to the presence of intense UV and cosmic ray fields. However, this radiation plays a fundamental role in the formation of molecules in both the gas phase and within the icy mantles of grains.[3–7] Cosmic rays are composed of 84% protons, 14% alpha particles, and the remaining 2% consisting of electrons, heavier nuclei, and exotic particles.[8] It is the lower energy sub-relativistic particles that penetrate and interact with the interior of the dense clouds.[9] At the same time, UV photons are also bombarding these regions. External UV fields are highly attenuated within the outer regions of dense cores, the smallest and densest types of molecular cloud where stars are born, and are weak in regions without stellar activity. However, this does not mean that radiation-induced chemistry does not occur within the deeper regions of these clouds. Cosmic rays have sufficient penetrating ability to produce secondary electrons that excite surrounding H_2 molecules into a higher electronic state. The resulting radiative decay produces Lyman and Werner band photons of fluxes of 10^4 photons cm^{-2} s^{-1}, which allows for chemical processes to occur even in the darkest of interstellar regions.[10] These secondary electrons (<50 eV) produced by cosmic rays can also directly ionize molecules and are proposed to be the primary driver of chemistry within the ice.[11–13] A single high energy (keV) electron can produce a cascade of hundreds to thousands of secondary electrons that can chemically or physically alter the ice.

Secondary electrons interact with condensed molecules in various ways: direct and indirect ionization, dissociative electron attachment, and neutral dissociation.[14,15] These events produce a wide range of highly reactive ions and radicals that undergo barrierless reactions via radical–radical, radical–ion, ion–molecule, and radical–molecule pathways.[3,6] The barrierless property is fundamental to explain the high chemical reactivity within the <10 K temperature regime in ices where astrochemically relevant reactions show non-Arrhenius behavior.[16,17] Early chemical models of

molecular clouds implemented these reactions in the gas phase to justify the abundances of various chemical species observed by infrared and radioastronomical observations. However, less than 80% of all molecular abundances could be reproduced with these models, and some errors were as large as a factor of 1000.[18] The abundance of the most important molecule in the interstellar medium (ISM), H_2, cannot be accounted for by gas-phase reactions alone because there is no efficient pathway for its production. However, the incorporation of solid phase grain chemistry more accurately reproduces the abundances of H_2 that is readily formed by hydrogen atom recombination on a dust grain surface.[19] Further development of astrochemical models has implemented cosmic ray and UV radiolysis pathways to obtain even more accurate models.[20] While the barrierless reactions between radicals and ions produced by interstellar radiation within the icy mantles of dust grains are essential to the formation of complex organic molecules (COMs) in the ISM, the underlying mechanisms involved in their synthesis are not yet fully understood. The pathways of formation become increasingly complex with increasing molecular size. This is in part due to the increasing number of possible conformers in which the molecule can exist, which increases by more than 3^n for n-alkanes, where n is the number of atoms in the molecular chain.[21]

The only way in which to directly measure conformer abundances in the ISM is through observational telescopes in the radio/microwave/mm-wave regime which capture the rotational spectra of molecules in the gas phase. COMs that have been formed through the energetic processing of icy grains may be released into the gas phase via thermal heating, photodesorption, chemical reactive desorption, sputtering, and spot heating from cosmic rays,[22–24] which may then be detected via rotational spectroscopy, in turn, yielding a structural fingerprint of the molecule observed. Extended line surveys with large single-dish telescopes and sophisticated data analysis have led to a burst of discovery of new molecules in recent years.[25,26] Of universal interest is the search for amino acids—although the simplest amino acid, glycine, remains elusive, its isomer, *syn*-glycolamide ($NH_2C(O)CH_2OH$), has recently been detected by Rivilla *et al.* with the Yebes 40 m and IRAM telescopes toward the G + 0.693–0.027 molecular cloud in the Sgr B2 region of the Galactic center.[27] The other $C_2H_5O_2N$ isomers, including the higher energy *anti* conformer of glycolamide and two conformers of glycine, were also included in this search. Although they were not detected, upper limits of their column densities were determined. The abundances of isomers observed could not be justified using only thermodynamic means but also required models incorporating radiation-induced non-equilibrium chemistry. The same story exists for the search for glyceraldehyde, a prerequisite sugar for the formation of RNA. It is an elusive fundamental prebiotic molecule that has several isomers detected in the ISM.[28] Discrepancies in isomer branching ratios of the formation of these molecules could be partially explained by investigating the conformer abundances of the reactants leading to the formation of larger COMs. Conformer-specific chemistry has been highlighted in processes involving alcohols, for example, where different vinyl alcohol conformers can lead to different product branching fractions in UV processed ices, as well as in calculated differences in hydrogen-abstraction reaction energies of the conformers of 1-propanol.[29,30] Considering that both sugars and amino acids in biological systems are homochiral, understanding the underlying pathways that lead to this observation is of great importance to astrobiologists. However, more laboratory experimentation is needed to support radioastronomical observations to understand how conformers affect these pathways.

Infrared spectroscopy has been the primary *in situ* technique for studying the effects of radiation on interstellar ice analogs.[31–36] Mass spectrometry with temperature-programmed desorption (TPD) or laser desorption experiments has also been conducted as both the primary measurement technique and a complement to IR spectroscopy to provide highly sensitive quantification of products from the irradiation of ices[37–47] with some isomer specificity using selective photoionization techniques.[48,49] Beyond this, vacuum ultraviolet (VUV) spectroscopy[50,51] and electron paramagnetic resonance[52] experiments have also been conducted to supplement IR spectroscopy. However, there are still limitations of these techniques that prevent unambiguous determination of the molecular abundances produced by the energetic processing of organic ices. Some of these limitations include structural isomers having similar ionization potentials that prevent selective measurement with PI-TOFMS, IR spectra and mass spectra becoming increasingly complex as the number of different species and their size increase, the influence of ice morphology on the IR spectra, and the inability to differentiate between conformers.

Rotational spectroscopy, on the other hand, provides an alternative detection method that yields a structure-specific spectrum for any species with at least a modest dipole moment. Coupling this approach with laboratory ice experiments is of interest not only because it affords unambiguous determination of molecular structure but also because it provides a direct comparison with the mm-wave/microwave detection used by radiotelescopes in astronomical observations. Rotational spectroscopy was first coupled with laboratory ice experiments by Yocum *et al.*[53] In their direct absorption approach, the ice samples were rapidly warmed and the chamber closed to the vacuum pumps in order to probe the gas phase molecules in the THz regime.[54] In doing so, the desorbed species are promptly thermalized via collisions with the 300 K chamber walls prior to detection. The inherent lack of sensitivity of rotational spectroscopy (in comparison with detection by mass spectrometry) is largely due to the way in which the rotational partition function scales with temperature, and has been the primary barrier to efficient coupling of this approach with ice desorption studies. While the use of THz detection is generally more favorable than the mm-waves employed here given the peak of the 300 K Boltzmann distribution for medium-sized molecules, this is vastly outweighed by the temperature dependence. For methanol at 25 K, for example, there is a factor of seven advantage for the buffer gas cooled molecules with mm-wave detection. For an astrobiologically relevant branched alkyl chained species, such as propyl cyanide, where conformer-specific desorption was previously reported,[55] it is more than a factor of 200.

Following the work of Yocum, Theulé *et al.*[56] demonstrated the application of *broadband* rotational spectroscopy to detect molecules desorbed from the interior of a waveguide. Chirped-pulse Fourier-transform rotational spectroscopy, developed by Brown *et al.* in 2008,[57] permits measurement of a spectrum >10 GHz in <1 us, allowing for several rotational transitions to be captured at once even in complex mixtures and, in turn, directly providing meaningful relative abundances of those species observed.

The instrument described in this article, Chirped-Pulse Ice (CPICE), overcomes the unfavorable temperature dependence of detection by rotational spectroscopy as well as the challenge of having a finite number of molecules contained within an ice sample (and in turn the limited averaging that may be performed in a single experiment) through the incorporation of a buffer gas cell (BGC) for prompt cooling to low temperature. The chirped-pulse detection employed affords quantification of isomers and conformers both within neat ices and within complex mixtures. Paper I of this series described the BGC component of CPICE in detail, and subsequent work highlights the conformer-specific desorption of *n*-propanol and *i*- and *n*-propyl cyanide ices recently observed.[58–60] In this article, we provide a detailed description of the full instrument including incorporation of the lower stage within this same UHV apparatus that allows for the generation of ices, their energetic processing, and the study of their sublimation via TPD.

This paper is organized as follows: Sec. II provides a brief summary of the buffer-gas cooling and mm-wave spectrometer components of this apparatus previously described in detail in paper I of this series[58] as well as a detailed description of the custom-built software employed to capture near-continuous broadband time-domain spectra over the course of a TPD experiment; Sec. III describes the lower stage used to generate ices not previously discussed; and Sec. IV describes the energetic processing tools that are employed in CPICE, including a high-energy electron gun and UV/VUV lamp; proof-of-principle experiments employing both are also described.

II. OVERVIEW OF CPICE

In CPICE, neat or energetically processed ices undergo sublimation via the slow warm-up process of TPD (1–5 K min^{-1}). The lower ice stage described below is raised, and the gas-phase species enter the 25 K BGC where they are promptly cooled via elastic collisions with Ne, leading to rapid translational equilibration at the cell temperature. Efficient translation-to-rotation coupling leads to rapid rotational cooling as well. The desorbed species are then detected by broadband rotational spectroscopy in the 60–90 GHz region. The mm-wave spectrometer employed to detect buffer gas cooled molecules via gas-phase injection in CPICE is described in detail in paper I of this series. Here, we briefly summarize minor additions to the hardware and describe the way in which our data acquisition software captures TPD data.

In ice experiments, a high duty-cycle average of time-domain free-induction decay signals is captured as a function of ice temperature at various ramping rates. A schematic view of this spectrometer is shown in Fig. 1. Here, excitation frequencies are generated by mixing signal from a pulsed arbitrary waveform generator (AWG, Keysight M8190A), which operates between DC and 5 GHz with a single-frequency local oscillator (LO) (Signal Core, 5511A) synthesizer output (100 MHz–20 GHz) using a triple-balanced mixer (Marki MM20530L). This chirp is amplified by a broadband low-noise amplifier (LNA, Miteq AMF-5D-00101200-23-10P) and isolated with a bandpass filter (BPFL) (Marki, FB0950). To obtain a frequency within the 60–90 GHz regime, the mixed signal is multiplied by eight using an active multiplier chain (AMC) (Quinstar, QMM-75301508-HDO1) before being emitted through a pyramidal standard gain horn (Quinstar, QWH-EPRR0). The expected power input to the standard gain horn is ~35 mW at 75 GHz. The emitted signal is collimated into the chamber using a plano-convex Teflon lens (ThorLabs LAT150) to reduce E-field loss before passing through the 1.5″ diameter sapphire window of the BGC. A comparison of signal intensities with and without the lens in this configuration results in ~7 times greater sensitivity. The down-conversion side of the spectrometer, highlighted in blue in Fig. 1, captures the subsequent molecular free-induction decay (FID) and down-converts the signal to be read by the data acquisition software. This molecular signal is transmitted from the BGC to the exterior of the chamber using a waveguide with one pyramidal standard gain

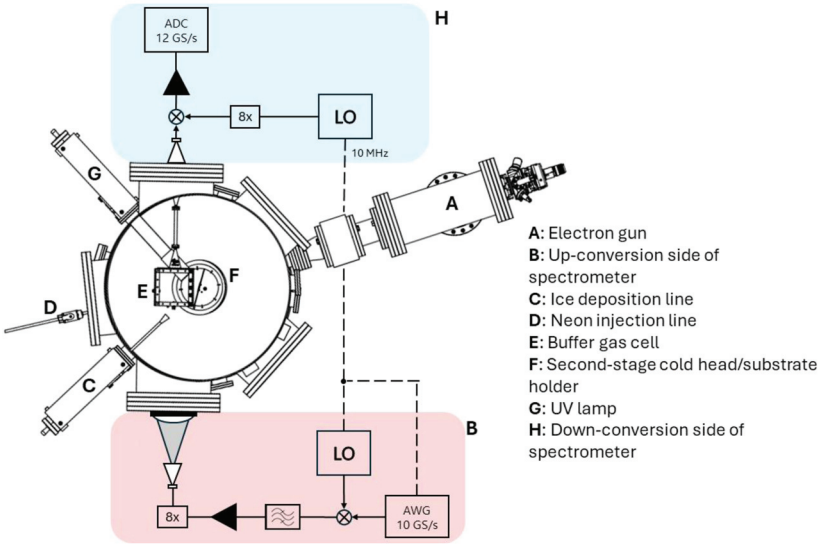

FIG. 1. Top–down view of the CPICE apparatus. The pink and blue-shaded regions encompass the up and down-conversion sides, respectively, of the mm-wave spectrometer.

horn fixed at each end. It is captured by a final pyramidal horn on the atmosphere side of the machine and mixed (Marki, MM20530L) with the output of a second LO (Signal Core, 5511A) that has passed through an 8× AMC (Quinstar, QMM-75301308D). The resulting mixed signal is down-converted between DC and 2.5 GHz to fit within the detectable range of the 10 GS/s data acquisition card (Acquiris, U5310A). Prior to reaching the card, it is amplified using a broadband low-gain amplifier (Mini-Circuits, ZJL-4G) to maximize the dynamic range of the available 1 V full-scale range of the DAC. The AWG and up-conversion LO are locked to a 10 MHz clock which is derived from the down-conversion LO synthesizer.

A custom LabView® program controls the data acquisition for the chirped pulse mm-wave spectrometer, as described in Ref. 58. Time-domain, downconverted FID signals associated with one or more programmable chirp patterns are signal averaged and logged for flexible subsequent analysis, in addition to real-time monitoring of the frequency domain spectra during the TPD measurements. A tradeoff between enhanced sensitivity and time resolution for a given temperature ramping rate is set by the number of FID acquisitions included in an average prior to Fourier transformation, where more averaging reduces the spectral amplitude noise at the expense of combining data measured over a longer time with a constantly ramping temperature. The data log of averaged FID signals typically included multiple blocks of 16k averages performed in the FPGA of the digitizer, co-added for several seconds in the computer before archiving. In a single-segment experiment, such as those described below, the corresponding 8 ms AWG period is replayed at a 125 kHz repetition rate and as such 125 K FIDs are acquired per second. At 16k samples per co-add, the digitizer transfers ~8 times per second. Further time-domain averaging could be performed offline from the data archive as needed, recognizing the range of temperatures over which the signals had been recorded.

III. GENERATION OF ICES

A. Lower stage coldhead

The lower stage cold head used for the generation of ices is based on the design of Jones and Kaiser.[48] As illustrated in Fig. 1, a closed-cycle helium cryostat (Sumitomo RDK415D2-F70L) is used to cool an oxygen-free high conductivity (OFHC) copper rod mounted to a rotatable (360°) bellows (Thermionics Vacuum Products, RNN-600/FA) and translatable (~8″) rotary seal (McCallister, BLT86-08) down to 4 K. Translation and rotation allows for the ice to be generated, characterized, and irradiated through the various ports located around the cylindrical chamber. This copper rod is surrounded by a cooled (27 K) OFHC radiation shield to prevent additional radiative heat loss. A 1″ × 1″ × 0.24″ Ag piece (Goodfellows 99.95% Ag) is thermally linked and housed near the top of the copper rod. The silver piece is machined with a polished 0.39″ × 0.39″ elevated face. A four-channel temperature controller (Lake Shore Model 336) is used to display the reading from two silicon diode temperature sensors (Lake Shore Cryotronics, DT-670-BO-QT32-2, uncalibrated, ±1 K accuracy). One sensor is located on the radiation shield ~7″ from the top of the substrate housing and records the temperature here. A second calibrated temperature sensor (Lake Shore Cryotronics, DT-670-BO-QT32-2, calibrated, ±0.1 K accuracy) is located ~0.5″ behind the silver substrate within the 4 K copper rod housing. A 50 Ω, 50 W, 0.25″ diameter cartridge heater (Lake Shore Cryotronics, HTR-50) is also located 0.5″ behind the silver substrate equidistant from the temperature sensor to regulate and ramp the substrate temperature for TPD experiments. The heater achieves a maximum linear temperature ramping rate of 5 K min^{-1} from 4 to >300 K. As the molecules reach their sublimation temperature, they desorb and travel 0.2″ to the 0.77″ diameter injection orifice of the BGC. The beam of desorbed molecules is perpendicular to the direction of the propagating excitation field. Based upon the solid angle of the aperture, ~50% of the sublimed molecules enter the cell to be measured.[58] The remaining molecules freeze out onto the face of the cold BGC. The controlled temperature ramping is achieved via the main CPICE program as described in Sec. II.

B. Gas deposition

In CPICE, ices are generated under UHV conditions (<1 × 10^{-10} Torr) and at ~ 4 K. To do so, gas phase samples are introduced into the chamber through 1/4″ stainless steel tubing that is evacuated with a roughing pump (Alcatel 2008A Direct Drive). The samples are subjected to a series of freeze/pump/thaw cycles as needed to remove any trapped volatiles prior to deposition, which is controlled by a high-precision VAT valve (VAT 59024-GE01). The deposition arm inside the UHV chamber is a straight 1/8″ ss tube that is connected to the VAT valve and has a flared 0.5″ diameter end located 1″ away from the silver 4 K surface. This deposition tube is connected to a UHV bellows (McAllister BLT27S-04) that can translate 4″ along the axis normal to the substrate to allow clearance after deposition to rotate the lower ice stage. The deposition arm is

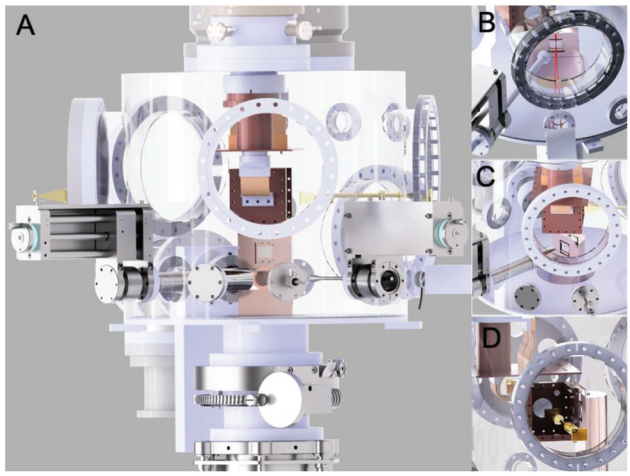

FIG. 2. Rendered drawing the CPICE apparatus. Panel A includes the entire UHV chamber within which the lower stage coldhead is used to generate ices and the upper coldhead is thermally linked to a BGC. The ports that surround the chamber are utilized in various ways as described in the main text. Panel B highlights the translatable arm used for the deposition of gases onto the cold Ag substrate while laser interferometry is performed to measure the thickness of the ice. Panel C illustrates the UV/VUV lamp fully contracted within the chamber to irradiate the ice. Panel D shows a side-view of the lower ice stage being raised to the BGC to perform TPD experiments. The perspective provided is from the down-conversion side where a series of horns and waveguides are used to direct the mm-wave FID out of the chamber and into the DAC.

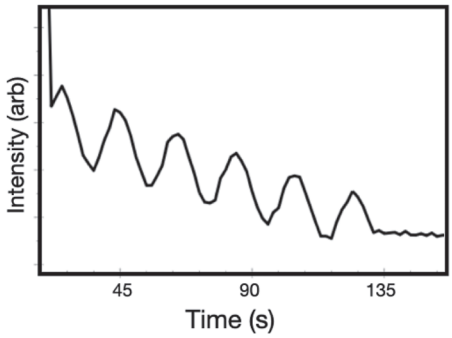

FIG. 3. Interference fringes used to determine the ice thickness of a CO + CH_4 ice.

~28° from the surface normal of the substrate to allow for the direct measurement of ice thickness during deposition.

The thickness of the ice is determined during deposition by laser interferometry. The reflection of an unpolarized HeNe laser (ThorLabs HNLS008R) from the cold silver surface is monitored during ice deposition with a photodiode (Thorlabs PM16-120). The laser beam enters and exits the chamber through a 2.75″ CF quartz window flange, and the angle of incidence is 1.5° at the silver surface. As the ice grows in thickness, the phase difference between the direct reflection from the ice surface and the light that has made a double-pass through the ice with a reflection at the silver surface will increase and produce cycles of constructive and destructive interference (Fig. 3). Successive maxima in the interference pattern are separated by the time it takes to increase the ice thickness by $\frac{\lambda}{2n \cos \theta}$

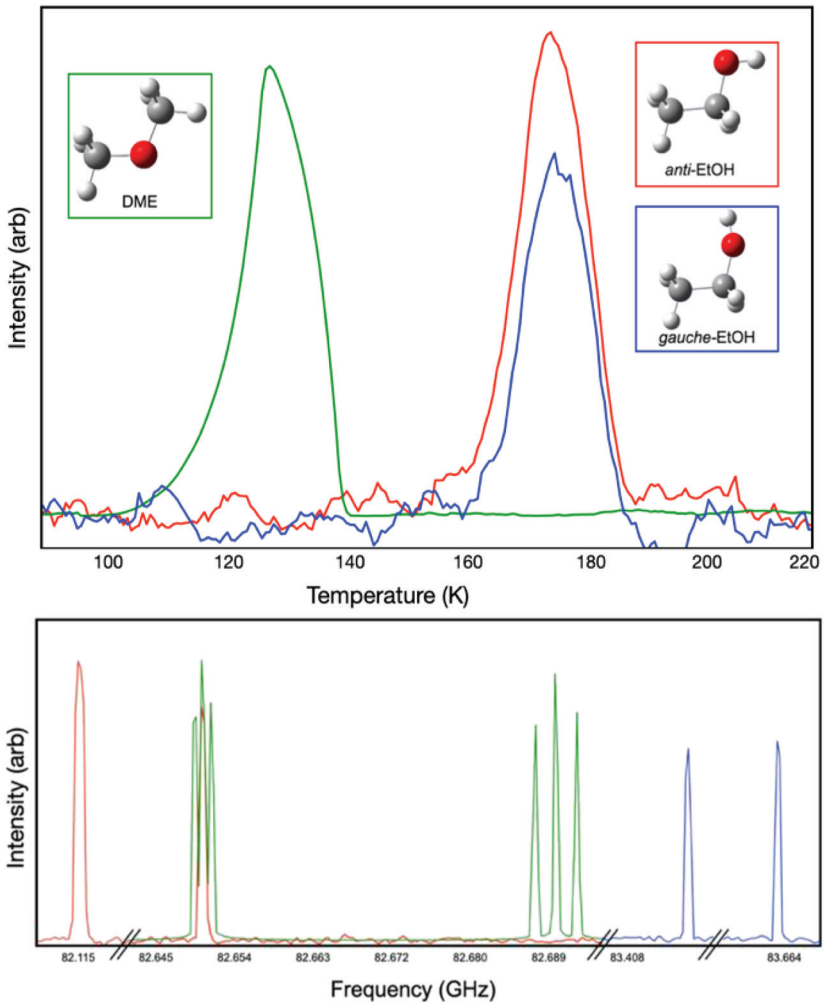

FIG. 4. Top: TPD spectra of DME, *anti* and *gauche*-EtOH. Bottom: broadband spectra from which the TPDs are derived.

with λ = 632.8 nm, the laser wavelength, n being the index of refraction of the ice, and θ being the angle of refraction, and the total film thickness can be calculated by counting the interference cycles,[61]

$$d = m * \left(\frac{\lambda}{2 * n * \cos \theta} \right), \quad (1)$$

where m is the number of cycles, λ is the wavelength of the incident light, n is the index of refraction of the ice, and θ is the angle of refraction (1.2°). Given our experimentally derived limit of detection (see Ref. 60) and consideration of the penetration depths of UV photons and 6 keV electrons, we typically generate ices of a few microns thick. Considering the density of a CO + CH_4 ice, for example, where the density is calculated using a linear relationship between the ice density and the fraction of each component, an ice of 50% CO (0.87 g/cm^3) and 50% CH_4 (0.47 g/cm^3) is estimated to be 0.67 g/cm^3[62,63] A 4 μm thick 1:1 CO:CH_4 ice on the 1 × 1cm^2 Ag substrate equates to a total of ~6.7 × 10^{16} molecules of the *parent* CO:CH_4 species.

Before outlining the way in which electron irradiation experiments are performed, we first provide broadband spectra from the TPD of unprocessed ices highlighting the structure-specific nature of the approach. Figure 4 includes broadband spectra of a 1:1 mixture of the isomers ethanol and dimethyl ether, as well as their TPD profiles generated over the course of a 2 K/min ramping rate. The *anti* and *gauche* conformers of ethanol are also resolved. The relative intensities of all species observed reflect a 25 K sample,[64] consistent with the temperature at which all species are detected within the BGC. Table I summarizes the frequencies and line strength factors (Sm^2) of the rotational transitions observed.

To gain a sense of the sensitivity in the current configuration, we can examine the signal-to-noise ratio (S/N) for direct gas phase injection of molecules. As we cannot state the density of molecules in the cell given rapid freeze out on the walls of an unknown fraction, instead we examine the signal at a given flow rate. At a flow of ~0.025 sccm or 6 × 10^{15} molecules/s into the cell, we obtain a S/N of 123 after 30 min of averaging for the anti-C_2H_5OH line at 82.115 GHz. We note the intensity of this line in the cell at 20 K is predicted to be 1700 times greater than the room temperature value of 2.9 × 10^{-6} nm2 MHz. The spectral resolution is fixed by the FID gate employed and limited by the T2 time and can be very long. In general, we employ shorter gate times to increase data throughput and do not need to push the resolution beyond 0.1 MHz. In these experiments, we employ a 4 μs long gate, corresponding to a resolution of 125 kHz.[64]

TABLE I. Rotational transitions of the molecular species observed with corresponding frequencies and Sμ^2 values.

Molecule	Frequency (GHz)	Transition	Sμ^2
anti EtOH	82.115	$3_{2,2}$–$3_{1,3}$	3.1
DME	82.649	$3_{1,3}$–$2_{0,2}$	13.7
anti EtOH	82.650	$11_{1,10}$–$11_{0,11}$	11.0
DME	82.650	$3_{1,3}$–$2_{0,2}$	54.8
DME	82.651	$3_{2,2}$–$3_{0,2}$	20.5
DME	82.686	$4_{2,2}$–$4_{1,3}$	8.0
DME	82.688	$4_{2,2}$–$4_{1,3}$	63.9
DME	82.691	$4_{2,2}$–$4_{1,3}$	24.0
gauche EtOH	83.417	$7_{0,7}$–$7_{1,7}$	11.2
gauche EtOH	83.662	$5_{1,4}$–$4_{1,4}$	8.3

IV. ENERGETIC PROCESSING OF ICES

In Secs. IV A and IV B, two proof-of-concept experiments are described. In both, the generation of H_2CO via energetic processing either by electron irradiation or UV/VUV photolysis is monitored over the course of TPD with detection by rotational spectroscopy in the mm-wave regime.

A. Electron irradiation

As shown in Fig. 1, CPICE is equipped with a high-energy electron gun (Kimball Physics EGG-3101C) (A) to study the energetic processing of ices via 100 eV–10 keV electrons. This gun is fitted with a standard refractory Ta cathode capable of producing emissions from 10 nA to 100 μA. A phosphor screen fitted to the top of the ice substrate housing is used to visualize and align the electron gun beam prior to irradiation.

To achieve a consistent energy dosage throughout an experiment, the electron beam output is monitored at the exit of the electron gun with a Faraday cup connected to a picoammeter. In this demonstration experiment, we chose to study mixed ices of CO and CH_4 given their significant reported abundances in the ISM (up to 85% and 11%, respectively, relative to water in low-mass stellar objects).[7] In addition to the abundance of the precursors, this system has shown the capability to produce COMs that have been observed in great abundance in the ISM as well. CO + CH_4 ices have been studied in detail following energetic processing leading to the detection of many products of astrochemical interest via photoionization mass spectrometry and FTIR. Such species include various alcohols, ethers, and carbonyls of varying complexity, many of which have been detected in the ISM.[48,49,65–69] We chose to investigate additional products of interest so that rotational spectroscopy could provide further insight on the chemistry of the system. In this work, we report the detection of H_2CO, which has not previously been observed in laboratory TPD experiments, since its ionization potential exceeds the photon energy in the photoionization mass spectrometers previously employed.[67] Rotational spectroscopy is quite sensitive for detection of H_2CO given its favorable partition function, highlighting the complementary nature of CPICE to the current suite of tools available to study ice chemistry in the laboratory.

We first briefly summarize the most probable chemical pathways for the synthesis of H_2CO from an energetically processed ice, before describing the specific parameters necessary to observe this species from the irradiation of CO and CH_4 in the CPICE apparatus.

Following high-energy electron irradiation, methane can directly dissociate through the following reaction:

$$CH_4 + CH_3 + H. \quad (2)$$

This process is the primary source of suprathermal hydrogen atoms within the ice that have sufficient kinetic energy to escape the matrix cage and diffuse through the ice. The hydrogen atom can

react with the CO present in the ice in a well-described successive hydrogenation pathway to form H_2CO,[70,71]

$$CO + H \rightarrow HCO, \quad (3)$$

$$HCO + H \rightarrow H_2CO. \quad (4)$$

This hydrogenation process will continue up to the formation of CH_3OH with H_2CO being an abundant intermediate. Future studies by CPICE across an expanded frequency range are currently underway to provide a global picture of the relative abundances of a wide range of synthesized organic species.

In these experiments, two depositions and irradiations were performed in a single experiment to maximize the total number density of energetically processed molecules. Each layer contained ~1.3 μm of the 1:1 CO:CH_4 mix and was irradiated for 1 h with a total electron flux of ~5×10^{11} cm^{-2} s^{-1}. In addition to a 30 min rest in between the first irradiation and second deposition, the ice rested for an additional 1 h at 4 K to allow for any chemistry to occur within the ice prior to beginning TPD. Following this energetic processing and rest period, the lower ice stage at 4 K was raised to the 25 K BGC. The ice temperature was then slowly ramped at a rate of 2 K/min. It is not until the lower ice stage reaches a temperature of 25 K that Ne gas is flowed into the BGC to prevent freeze-out of the Ne onto the lower ice stage. The optimal cooling condition established for TPD experiments is slightly less than that identified following gas phase injection from a room temperature sample.[57] A temperature ramp of 5 K/min then begins with mm-wave excitation of the $J = 1_{0,1}–0_{0,0}$ transition of H_2CO at 72.8379 GHz. The frequency-domain spectrum of the transition observed between ~110 and 140 K is inset within Fig. 5. The TPD profile captures the intensity of this transition as a function of temperature. It may subsequently be compared to that which is observed under this same condition in the absence of exposure to electron irradiation (blue trace in Fig. 5). The previously described single-frequency $\frac{\pi}{2}$ pulse condition was employed in these experiments to maximize sensitivity.[59] The experimentally derived pulse duration was 1 μs with a listening time of 4.5 μs, which exceeds the T2 dephasing time of H_2CO under the experimental conditions employed.

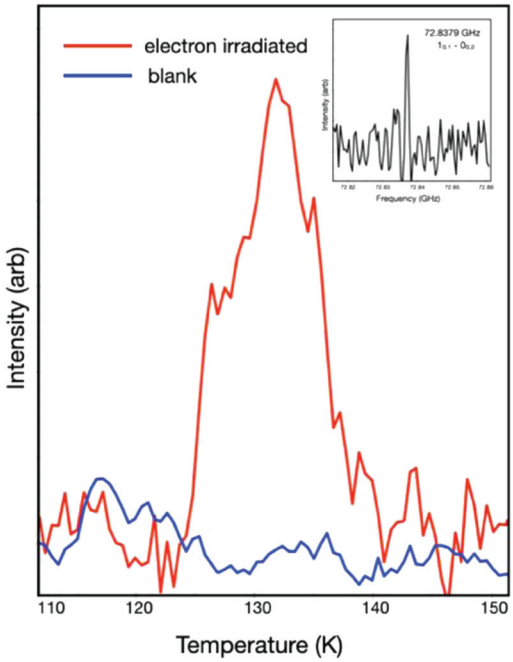

FIG. 5. TPD spectrum of H_2CO generated from electron irradiation of a CH_4 + CO ice (red). In blue is a non-irradiated ice probing this same frequency over the course of TPD (blue).

B. UV/VUV irradiation

In addition to an electron gun, CPICE is also equipped with a UV/VUV deuterium lamp (Hamamatsu L10706) for energetic processing studies. The spectral distribution covers 120–165 nm (10.3–7.5 eV) with 80% irradiance at 160 nm and 20% irradiance at 120 nm with peak irradiance being 0.14 μW cm^{-2} nm^{-1} @ 160 nm. Within the entire 120–160 nm wavelength region, the photon flux is $\varphi = 10^{15}$ photons cm^{-2} s^{-1}. This lamp is attached to a 4″ linear translatable bellows (McAllister BLT27S-04) on one of the 2.75″ CF flanges on the main chamber facing the ice surface. When fully inserted within the UHV chamber, the UV/VUV lamp is ~2″ away from the ice (see Fig. 2, Panel C). The area of the output window of the lamp is 1.3 cm^2, with an incidence angle of 7.5°, resulting in a total beam area of 5.3 cm^2 at the surface of the ice. The penetration depth of VUV photons is expected to be similar to keV electrons, but the energy distribution within the ice is different for photons and is dependent upon the optical cross-section of the irradiated species.[3]

Here, we again demonstrate the detection of H_2CO, in this case from the UV/VUV irradiation of neat methanol ice. On the basis of previously determined rate coefficients in methanol photodissociation,[72] the most favorable pathway to production of H_2CO is through the methoxy intermediate (CH_3O) rather than the hydroxymethyl radical (CH_2OH). This pathway, in addition to the one-step route from the unimolecular decomposition of methanol itself are the primary mechanisms involved in H_2CO formation based upon previous reports.

In these demonstration experiments, neat methanol ice was deposited at 4 K following a series of freeze–pump–thaw cycles. Three depositions of 3 mm thick ices were performed (yielding a total thickness of ~ 9 μm). Each deposition was irradiated for 1 h followed by a 30 min rest time. The penetration depth of our VUV beam within our methanol ice is estimated using the Beer–Lambert law. The max penetration depth of the ice is taken to be when the incident VUV beam is attenuated by 99%. Given the average optical cross section of methanol ice in the 120–165 nm range (9×10^{-18} cm^{-2} $molecule^{-1}$)[73] and the density of the methanol ice at 20 K (0.636 g cm^{-3}),[74] the maximum penetration depth is 0.4 μm. The same procedure as described above for raising the lower ice stage to the BGC, turning on the 4 sccm Ne flow, and ramping the temperature at a rate of 5 K/min was employed. The resulting TPD is shown in Fig. 6, again probing the same H_2CO transition at 72.8379 GHz. The signal in these experiments is first observed at a slightly lower desorption temperature in comparison with that from the CH_4 + CO electron irradiation experiments. This is expected given the different parent ice composition and thicknesses, irradiation sources, and VUV/UV photon vs 6 keV electron flux.

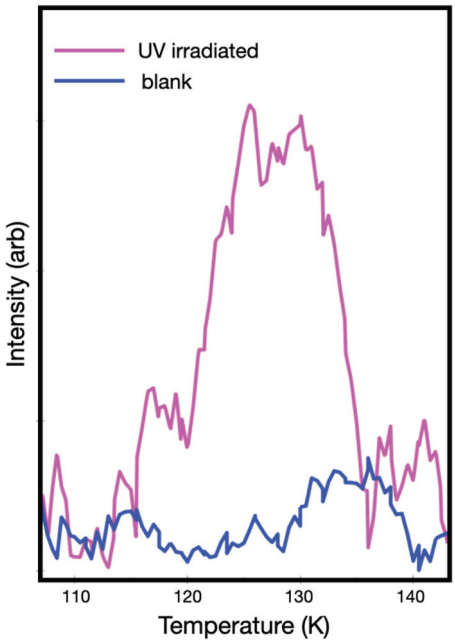

FIG. 6. TPD spectrum of H_2CO generated from UV irradiation of a methane ice (pink) in addition to a non-irradiated ice probing this same frequency over the course of TPD (blue).

V. CONCLUSION

This article is the second in a series of two that describes an apparatus to probe the desorbed chemical products formed in energetically processed ices, using TPD followed by buffer gas cooling and chirped-pulse rotational spectroscopy in the 60–90 GHz regime. In the proof-of-principle experiments described above, we observe H_2CO in the gas phase following TPD of a methanol ice subjected to UV/VUV photons, as well as a 6 keV electron irradiated 1:1 CO + CH_4 ice mixture. Building upon our previous desorption studies highlighting conformer-specific sublimation in neat ices, experiments are currently underway, which take advantage of the unique capabilities of CPICE to explore the chemistry underlying the formation of branched-chain COMs, specifically for those systems that are proposed to have highly conformer- and isomer-specific pathways to their synthesis. Separate experiments in CPICE examining sublimation dynamics are also underway. Here, we observe non-equilibrium effects over the course of TPD, where the measured vibrational temperature of the desorbed species is less than the temperature of desorption.

ACKNOWLEDGMENTS

B.M.B. gratefully acknowledged the University of Missouri for generous startup funds, NSF Engineering, Grant No. 2314347, and NSF Chemistry, Grant No. 2414316. The authors also thanked David Patterson and Lincoln Satterthwaite for their suggestions on the BGC design, as well as Ralf Kaiser and Andrew Turner for their feedback on the lower stage components used for the generation of ices. The contributions of G.E.H., as a senior scientist emeritus at BNL, have not been directly supported by any specific BNL or DOE funded program.

AUTHOR DECLARATIONS

Conflict of Interest

The authors have no conflicts to disclose.

Author Contributions

T. J. Hager: Data curation (equal); Formal analysis (equal); Investigation (equal); Writing – original draft (lead). **B. M. Moore**: Data curation (equal); Formal analysis (equal); Investigation (equal); Writing – review & editing (equal). **Q. D. Borengasser**: Data curation (equal); Formal analysis (equal); Investigation (equal). **A. C. Kanaherarachchi**: Data curation (equal); Formal analysis (equal); Investigation (equal). **K. T. Renshaw**: Data curation (equal); Formal analysis (equal); Investigation (equal). **S. Radhakrishnan**: Resources (equal). **G. E. Hall**: Resources (equal); Software (lead); Writing – review & editing (equal). **B. M. Broderick**: Conceptualization (lead); Formal analysis (equal); Funding acquisition (equal); Project administration (lead); Supervision (lead); Writing – review & editing (equal).

DATA AVAILABILITY

The data that support the findings of this study are available from the corresponding author upon reasonable request.

REFERENCES

[1]B. A. McGuire, "2021 census of interstellar, circumstellar, extragalactic, protoplanetary disk, and exoplanetary molecules," Astrophys. J. Suppl. Ser. **259**(2), 30 (2021).
[2]E. Herbst and E. F. van Dishoeck, "Complex organic interstellar molecules," Annu. Rev. Astron. Astrophys. **47**, 427–480 (2009).
[3]K. I. Öberg, "Photochemistry and astrochemistry: Photochemical pathways to interstellar complex organic molecules," Chem. Rev. **116**(17), 9631–9663 (2016).
[4]C. N. Shingledecker and E. Herbst, "A general method for the inclusion of radiation chemistry in astrochemical models," Phys. Chem. Chem. Phys. **20**(8), 5359–5367 (2018).
[5]H. J. Fraser, M. R. S. McCoustra, and D. A. Williams, "The molecular universe," Astron. Geophys. **43**(2), 2.10–2.18 (2002).
[6]C. R. Arumainayagam, R. T. Garrod, M. C. Boyer, A. K. Hay, S. T. Bao, J. S. Campbell, J. Wang, C. M. Nowak, M. R. Arumainayagam, and P. J. Hodge, "Extraterrestrial prebiotic molecules: Photochemistry *vs.* radiation chemistry of interstellar ices," Chem. Soc. Rev. **48**(8), 2293–2314 (2019).
[7]A. A. Boogert, P. A. Gerakines, and D. C. B. Whittet, "Observations of the icy universe," Annu. Rev. Astron. Astrophys. **53**(1), 541–581 (2015).
[8]I. A. Grenier, J. H. Black, and A. W. Strong, "The nine LIves of cosmic rays in galaxies," Annu. Rev. Astron. Astrophys. **53**, 199–246 (2015).
[9]M. Padovani, A. V. Ivlev, D. Galli, S. S. R. Offner, N. Indriolo, D. Rodgers-Lee, A. Marcowith, P. Girichidis, A. M. Bykov, and J. M. D. Kruijssen, "Impact of low-energy cosmic rays on star formation," Space Sci. Rev. **216**(2), 29 (2020).
[10]S. S. Prasad and S. P. Tarafdar, "UV radiation field inside dense clouds: Its possible existence and chemical implications," Astrophys. J. **267**, 603–609 (1983).

[11]Q. T. Wu, H. Anderson, A. K. Watkins, D. Arora, K. Barnes, M. Padovani, C. N. Shingledecker, C. R. Arumainayagam, and J. B. R. Battat, "Role of low-energy (<20 eV) secondary electrons in the extraterrestrial synthesis of prebiotic molecules," ACS Earth Space Chem. **8**, 79–88 (2023).
[12]M. C. Boyer, N. Rivas, A. A. Tran, C. A. Verish, and C. R. Arumainayagam, "The role of low-energy (≤20 eV) electrons in astrochemistry," Surf. Sci. **652**, 26–32 (2016).
[13]C. R. Arumainayagam, H. Lee, R. B. Nelson, D. R. Haines, and R. P. Gunawardane, "Low-energy electron-induced reactions in condensed matter," Surf. Sci. Rep. **65**(1), 1–44 (2010).
[14]F. Schmidt, T. Borrmann, M. P. Mues, S. Benter, P. Swiderek, and J. H. Bredehöft, "Mechanisms of electron-induced chemistry in molecular ices," Atoms **10**(1), 25 (2022).
[15]S. M. Pimblott and J. A. Laverne, "Effect of electron energy on the radiation chemistry of liquid water," Radiat. Res. **150**(2), 159–169 (1998).
[16]I. R. Sims, "Tunnelling in space," Nat. Chem. **5**(9), 734–736 (2013).
[17]V. Aquilanti, N. D. Coutinho, and V. H. Carvalho-Silva, "Kinetics of low-temperature transitions and a reaction rate theory from non-equilibrium distributions," Philos. Trans. R. Soc. A **375**(2092), 20160201 (2017).
[18]R. Garrod, I. Hee Park, P. Caselli, and E. Herbst, "Are gas-phase models of interstellar chemistry tenable? The case of methanol," Faraday Discuss. **133**, 51–62 (2006).
[19]H. B. Perets, O. Biham, G. Manico, V. Pirronello, J. Roser, S. Swords, and G. Vidali, "Molecular hydrogen formation on ice under interstellar conditions," Astrophys. J. **627**, 850 (2005).
[20]A. Paulive, C. N. Shingledecker, and E. Herbst, "The role of radiolysis in the modelling of $C_2H_4O_2$ isomers and dimethyl ether in cold dark clouds," Mon. Not. R. Astron. Soc. **500**(3), 3414–3424 (2020).
[21]H. Goto, E. Osawa, and M. Yamato, "How many conformers are there for small *n*-alkanes? Consequences of asymmetric deformation in GG′ segment," Tetrahedron **49**(2), 387–396 (1993).
[22]P. Boduch, E. Dartois, A. L. F. de Barros, E. F. da Silveira, A. Domaracka, X. Lv, M. E. Palumbo, S. Pilling, H. Rothard, E. S. Duarte, and G. Strazzulla, "Radiation effects in astrophysical ices," J. Phys.: Conf. Ser. **629**(1), 012008 (2015).
[23]A. V. Ivlev, T. B. Rocker, A. Vasyunin, and P. Caselli, "Impulsive spot heating and thermal explosion of interstellar grains revisted," Astrophys. J. **805**(1), 59 (2015).
[24]L. B. d'Hendecourt, L. J. Allamandola, F. Baas, and J. M. Greenberg, "Interstellar grain explosions: Molecule cycling between gas and dust," Astron. Astrophys. **109**(2), L12–L14 (1982).
[25]M. Guélin and J. Cernicharo, "Organic molecules in interstellar space: Latest advances," Front. Astron. Space Sci. **9**, 787567 (2022).
[26]M. K. McClure, W. R. M. Rocha, K. M. Pontoppidan, N. Crouzet, L. E. U. Chu, E. Dartois, T. Lamberts, J. A. Noble, Y. J. Pendleton, G. Perotti *et al.*, "An Ice Age JWST inventory of dense molecular cloud ices," Nat. Astron. **7**, 431–443 (2023).
[27]V. M. Rivilla, M. Sanz-Novo, I. Jiménez-Serra, J. Martín-Pintado, L. Colzi, S. Zeng, A. Megías, Á. López-Gallifa, A. Martínez-Henares, S. Massalkhi *et al.*, "First glycine isomer detected in the interstellar medium: Glycolamide ($NH_2C(O)CH_2OH$)," Astrophys. J. Lett. **953**(2), L20 (2023).
[28]V. M. Rivilla, L. Colzi, I. Jiménez-Serra, J. Martín-Pintado, A. Megías, M. Melosso, L. Bizzocchi, Á. López-Gallifa, A. Martínez-Henares, S. Massalkhi *et al.*, "Precursors of the RNA world in space: Detection of (Z)-1,2-ethenediol in the interstellar medium, a key intermediate in sugar formation," Astrophys. J. Lett. **929**(1), L11 (2022).
[29]D. Rösch, G. H. Jones, R. Almeida, R. L. Caravan, A. Hui, A. W. Ray, C. J. Percival, S. P. Sander, M. D. Smarte, F. A. F. Winiberg *et al.*, "Conformer-dependent chemistry: Experimental product branching of the vinyl alcohol + OH + O_2 reaction," J. Phys. Chem. A **127**(14), 3221–3230 (2023).
[30]D. Troya, "Reactivity consequences of conformational isomerism in 1-propanol," J. Phys. Chem. A **123**(5), 1044–1050 (2019).
[31]L. J. Allamandola, S. A. Sandford, and G. J. Valero, "Photochemical and thermal evolution of interstellar/precometary ice analogs," Icarus **76**(2), 225–252 (1988).
[32]P. V. Zasimov, E. V. Sanochkina, and V. I. Feldman, "Radiation-induced transformations of acetaldehyde molecules at cryogenic temperatures: A matrix isolation study," Phys. Chem. Chem. Phys. **24**(1), 419–432 (2022).
[33]F. Freitas and S. Pilling, "Laboratory investigation of X-ray photolysis of methanol ice and its implication on astrophysical environments," Quím. Nova **43**(5), 521–527 (2020).
[34]R. L. Hudson and M. H. Moore, "Far-IR spectral changes accompanying proton irradiation of solids of astrochemical interest," Radiat. Phys. Chem. **45**(5), 779–789 (1995).
[35]P. A. Gerakines, W. A. Schutte, and P. Ehrenfreund, "Ultraviolet processing of interstellar ice analogs. I. Pure ices," Astron. Astrophys. **312**, 289–305 (1995).
[36]P. Modica and M. E. Palumbo, "Formation of methyl formate after cosmic ion irradiation of icy grain mantles," Astron. Astrophys. **519**, A22 (2010).
[37]M. Bulak, D. M. Paardekooper, G. Fedoseev, and H. Linnartz, "Photolysis of acetonitrile in a water-rich ice as a source of complex organic molecules: CH_3CN and H_2O:CH_3CN ices," Astron. Astrophys. **647**, A82 (2021).
[38]S. E. Bisschop, G. W. Fuchs, E. F. Van Dishoeck, and H. Linnartz, "H-atom bombardment of CO_2, HCOOH, and CH_3CHO containing ices," Astron. Astrophys. **474**(3), 1061–1071 (2007).
[39]T. Butscher, F. Duvernay, G. Danger, and T. Chiavassa, "Radical-induced chemistry from VUV photolysis of interstellar ice analogues containing formaldehyde," Astron. Astrophys. **593**, A60 (2016).
[40]N. A. Mrad, F. Duvernay, T. Chiavassa, and G. Danger, "Methanol ice VUV photoprocessing: GC-MS analysis of volatile organic compounds," Mon. Not. R. Astron. Soc. **458**(2), 1234–1241 (2016).
[41]B. L. Henderson and M. S. Gudipati, "Direct detection of complex organic products in ultraviolet (Lyα) and electron-irradiated astrophysical and cometary ice analogs using two-step laser ablation and ionization mass spectrometry," Astrophys. J. **800**(1), 66 (2015).
[42]M. S. Akerman, H. Iny, R. Sagi, and M. Asscher, "Chemical reactivity of strongly interacting, hydrogen-bond-forming molecules following 193 nm photon irradiation: Methanol in amorphous solid water at low temperatures," Langmuir **39**(7), 2838–2849 (2023).
[43]R. Martín-Doménech, G. M. Muñoz Caro, and G. A. Cruz-Díaz, "Study of the photon-induced formation and subsequent desorption of CH_3OH and H_2CO in interstellar ice analogs," Astron. Astrophys. **589**, A107 (2016).
[44]K. I. Öberg, R. T. Garrod, E. F. Van Dishoeck, and H. Linnartz, "Formation rates of complex organics in UV irradiated CH_3OH-rich ices," Astron. Astrophys. **504**(3), 891–913 (2009).
[45]P. Herczku, D. V. Mifsud, S. Ioppolo, Z. Juhász, Z. Kaňuchová, S. T. S. Kovács, A. Traspas Muiña, P. A. Hailey, I. Rajta, I. Vajda *et al.*, "The ice chamber for astrophysics–astrochemistry (ICA): A new experimental facility for ion impact studies of astrophysical ice analogs," Rev. Sci. Instrum. **92**(8), 084501 (2021).
[46]K. A. Kipfer, A. Galli, A. Riedo, M. Tulej, P. Wurz, and N. F. Ligterink, "Complex ice chemistry: A comparative study of electron irradiated planetary ice analogues containing methane," Icarus **410**, 115742 (2024).
[47]H. J. Fraser, M. P. Collings and M. McCoustra, "Laboratory surface astrophysics experiment," Rev. Sci. Instrum. **73**, 2161–2170 (2002).
[48]B. M. Jones and R. I. Kaiser, "Application of reflectron time-of-flight mass spectroscopy in the analysis of astrophysically relevant ices exposed to ionization radiation: Methane (CH_4) and D4-methane (CD_4) as a case study," J. Phys. Chem. Lett. **4**(11), 1965–1971 (2013).
[49]A. M. Turner and R. I. Kaiser, "Exploiting photoionization reflectron time-of-flight mass spectrometry to explore molecular mass growth processes to complex organic molecules in interstellar and solar system ice analogs," Acc. Chem. Res. **53**(12), 2791–2805 (2020).
[50]R. L. James, S. Ioppolo, S. V. Hoffmann, N. C. Jones, N. J. Mason, and A. Dawes, "Systematic investigation of CO_2: NH_3 ice mixtures using mid-IR and VUV spectroscopy – Part 1: Thermal processing," RSC Adv. **10**(61), 37515–37528 (2020).
[51]R. L. James, S. Ioppolo, S. V. Hoffmann, N. C. Jones, N. J. Mason, and A. Dawes, "Systematic investigation of CO_2: NH_3 ice mixtures using mid-IR and VUV spectroscopy – Part 2: Electron irradiation and thermal processing," RSC Adv. **11**(52), 33055–33069 (2021).
[52]V. I. Feldman, "Structure and properties of hydrocarbon radical cations in low-temperature matrices as studied by a combination of EPR and IR spectroscopy," Acta Chem. Scand. **51**, 181–192 (1997).

[53]K. M. Yocum, O. H. Wilkins, J. C. Bardwell, S. N. Milam, and P. A. Gerakines, "Gas-phase ortho-to-para ratio of formaldehyde formed at low temperatures in laboratory ices," Astrophys. J. Lett. **958**, L41 (2023).
[54]K. M. Yocum, H. H. Smith, E. W. Todd, L. Mora, P. A. Gerakines, S. N. Milam, and S. L. Widicus Weaver, "Millimeter/submillimeter spectroscopic detection of desorbed ices: A new technique in laboratory astrochemistry," J. Phys. Chem. A **123**(40), 8702–8708 (2019).
[55]A. Kanaherarachchi, T. Hager, Q. Borengasser, and B. M. Broderick, "Conformer distributions of *n*-propyl cyanide in the gas phase and following ice sublimation measured by broadband rotational spectroscopy," ACS Earth Space Chem. **8**(1), 14–20 (2024).
[56]P. Theulé, C. Endres, M. Hermanns, J.-B. Bossa, and A. Potapov, "High-resolution gas phase spectroscopy of molecules desorbed from an ice surface: A proof-of-principle study," ACS Earth Space Chem. **4**(1), 86–91 (2020).
[57]G. G. Brown, B. C. Dian, K. O. Douglass, S. M. Geyer, S. T. Shipman, and B. H. Pate, "A broadband Fourier transform microwave spectrometer based on chirped pulse excitation," Rev. Sci. Instrum. **79**(5), 053103 (2008).
[58]S. Radhakrishnan, T. Hager, A. Kanaherarachchi, C. Williams, G. E. Hall, and B. M. Broderick, "Buffer gas cooled ice chemistry. I. Buffer gas cell and mm-wave spectrometer," J. Chem. Phys. **157**, 154201 (2022).
[59]Q. Borengasser, T. Hager, A. Kanaherarachchi, D. Troya, and B. M. Broderick, "Conformer-specific desorption in propanol ices probed by chirped-pulse millimeter-wave rotational spectroscopy," J. Phys. Chem. Lett. **14**(29), 6550–6555 (2023).
[60]R. M. Gurusinghe, N. Dias, and B. M. Broderick, "Buffer gas cooling for sensitive rotational spectroscopy of ice chemistry: A proposal," Chem. Phys. Lett. **762**, 138125 (2021).
[61]R. Brunetto, G. Caniglia, G. A. Baratta, and M. E. Palumbo, "Integrated near-infrared band strengths of solid CH_4 and its mixtures with N_2," Astrophys. J. **686**(2), 1480–1485 (2008).
[62]R. Luna, M. Ángel Satorre, M. Domingo, C. Millan, and C. Santonja, "Density and refractive index of binary CH_4, N_2, and CO_2 ice mixtures," Icarus **221**(1), 186–191 (2012).
[63]R. Luna, C. Millán, M. Domingo, C. Santonja, and M. Á. Satorre, "Density and refractive index of carbon monoxide ice at different temperatures," Astrophys. J. **935**(2), 134 (2022).
[64]H. S. P. Muller, F. Schloder, J. Stutzki, and G. Winnewisser, "The cologne database for molecular spectroscopy, CDMS: A useful tool for astronomers and spectroscopists," J. Mol. Struct. **742**, 215–227 (2005).
[65]C. J. Bennett, C. S. Jamieson, Y. Osamura, and R. I. Kaiser, "A combined experimental and computational investigation on the synthesis of acetaldehyde [$CH_3CHO(X^1A')$] in interstellar ices," Astrophys. J. **624**(2), 1097–1115 (2005).
[66]R. I. Kaiser, S. Maity, and B. M. Jones, "Infrared and reflectron time-of-flight mass spectroscopic analysis of methane (CH_4)–carbon monoxide (CO) ices exposed to ionization radiation – Toward the formation of carbonyl-bearing molecules in extraterrestrial ices," Phys. Chem. Chem. Phys. **16**(8), 3399–3424 (2014).
[67]M. J. Abplanalp, M. Förstel and R. I. Kaiser, "Exploiting single photon vacuum ultraviolet photoionization to unravel the synthesis of complex organic molecules in interstellar ices," Chem. Phys. Lett. **644**, 79–98 (2016).
[68]M. J. Abplanalp and R. I. Kaiser, "On the formation of complex organic molecules in the interstellar medium: Untangling the chemical complexity of carbon monoxide–hydrocarbon containing ice analogues exposed to ionizing radiation *via* a combined infrared and reflectron time-of-flight analysis," Phys. Chem. Chem. Phys. **21**(31), 16949–16980 (2019).
[69]C. Zhu, H. Wang, I. Medvedkov, J. Marks, M. Xu, J. Yang, T. Yang, Y. Pan, and R. I. Kaiser, "Exploitation of synchrotron radiation photoionization mass spectrometry in the analysis of complex organics in interstellar model ices," J. Phys. Chem. Lett. **13**(30), 6875–6882 (2022).
[70]D. Woon, "Modeling gas-grain chemistry with quantum chemical cluster calculations. I. Heterogeneous hydrogenation of CO and H_2CO on icy grain mantles," Astrophys. J. **569**(1), 541–548 (2002).
[71]G. W. Fuchs, H. M. Cuppen, S. Ioppolo, C. Romanzin, S. E. Bisschop, S. Andersson, E. F. Van Dishoeck, and H. Linnartz, "Hydrogenation reactions in interstellar CO ice analogues: A combined experimental/theoretical approach," Astron. Astrophys. **505**(2), 629–639 (2009).
[72]C. J. Bennett, S. Chen, B. Sun, A. H. H. Chang, and R. I. Kaiser, "Mechanistical studies on the irradiation of methanol in extraterrestrial ices," Astrophys. J. **660**, 1588 (2007).
[73]B. Cheng, M. Bahou, W. Chen, C. Yui, Y. Lee, and L. Lee, "Experimental and theoretical studies on vacuum ultraviolet absorption cross sections and photodissociation of CH_3OH, CH_3OD, CD_3OH, and CD_3OD," J. Chem. Phys. **117**, 1633–1640 (2002).
[74]R. Luna, G. Molpeceres, J. Ortigoso, M. Satorre, M. Domingo, and B. Mate, "Densities, infrared band strengths, and optical constants of solid methanol," Astron. Astrophys. **617**, A116 (2018).